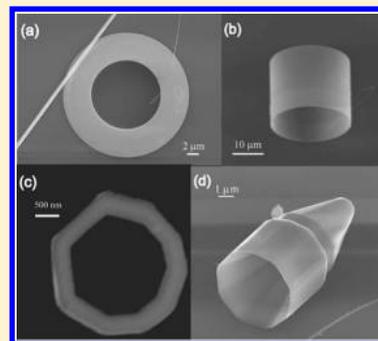# Polyhedral Topological Crystals

Masakatsu Tsubota,*,† Katsuhiko Inagaki,‡ Toru Matsuura,§ and Satoshi Tanda†,‖

†Department of Applied Physics and ‖Center of Education and Research for Topological Science and Technology, Hokkaido University, Sapporo 060-8628, Japan

‡Department of Physics, Asahikawa Medical University, Asahikawa 078-8510, Japan

§Creative Research Institute, Research Department, Hokkaido University, Sapporo 001-0021, Japan

ABSTRACT: We have synthesized micrometer-scale polyhedral ring crystals of TaS_3 by the chemical vapor transportation method. The polyhedral ring crystals are closed-loop crystals with several vertices. We investigated the crystallinity and flatness of the facets by the electron backscatter diffraction technique and found that the orientation of the crystal axis changed abruptly at several points. Observing the size of the crystals, we found a new phase of topological crystals and propose a phase diagram of ring-polyhedral crystals in terms of radius and thickness. We also propose a mechanism of polygonization in which the vertices of the polyhedral crystals are formed from concentrated dislocations as a result of distance-dependent interactions between them.

■ INTRODUCTION

Recently, there has been increasing interest in loop nanostructures and microstructures.[1−3] Theoretical and experimental attention has been paid to crystals of these structures.[4−7] Topological crystals were discovered in 2000[8] and have been researched since then. First, a $NbSe_3$ ring crystal was synthesized together with whisker crystals. Next, other topological crystals (Möbius-strip-, figure-eight-, and Hopf-link-shaped crystals) were discovered,[9,10] and then topological crystals of other compounds ($TaSe_3$,[11] TaS_3,[12] and NbS_3[13]) were discovered. Crystal topology broke through a new stage of understanding of physical phenomena.[12,14,15]

Topological crystals are conceptually different from conventional crystals. A crystal is constructed by the infinite repetition of atoms, as shown in Figure 1 (left). As a result, a conventional crystal displays discrete translational and rotational symmetries, and its crystal lattices can be mapped onto itself by translational symmetry or by various other symmetry operations. On the other hand, a topological crystal does not display discrete translational or rotational symmetries, because the orientation of the crystal axes is smoothly changing. This also indicates that the distribution of dislocations/disclinations introduced into a topological crystal [as shown in Figure 1 (right)] must be smooth.[16,17] When a topological crystal needs to be bent, geometrical frustration is relaxed through the inclusion of edge dislocations, and other types of dislocations, such as screw and mixed dislocations, do not need to be considered.[18−20] However, the interplay between the global topology of the crystals and the distribution of dislocations/disclinations is still unclear.

In this article, we report a new type of topological crystals having several vertices in the tantalum trisulfied (TaS_3) system. Using the electron backscatter diffraction technique, we confirmed the crystallinity and flatness of the facets in ring and polyhedral crystals of TaS_3 and then found that the orientation of the crystal axes on the polyhedral ring crystals changes abruptly at several points. To reveal the growth mechanism of the polyhedral crystals, we investigated several topological crystals in terms of radius and width. From the radius—width diagram, we propose a phase diagram of smooth to polyhedral topological crystals, based on that predicted by Hayashi et al.[21]
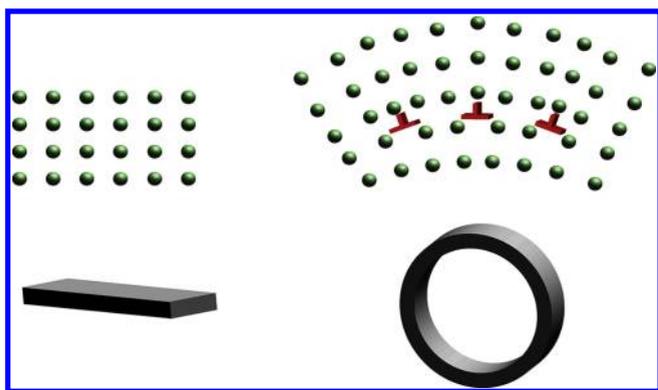
■ EXPERIMENTAL METHODS

The polyhedral ring-crystal samples of TaS_3 were synthesized by the chemical vapor transport (CVT) method. We enclosed the starting materials (a tantalum wire and sulfur powder in a mole ratio of 1:3) in an evacuated quartz tube. The tube was heated in a furnace with a temperature gradient. The temperature of the furnace was set at 560 °C on one side and 600 °C on the other side. The tube was put in the furnace for several hours, with the starting material on the high-temperature side. The grain crystals of Ta or TaS_3 were transported to the low-temperature side by convection and grew into crystals there. After several hours, we picked up the tube and quenched its high-temperature side in liquid nitrogen because this prevents sulfur from adhering to the quartz tube. We obtained conventional whisker (needlelike) crystals, ring/tube crystals, and polyhedral ring crystals.

■ RESULTS

We previously discovered polyhedral topological crystals in MX_3 (M = transition metal, X = chalcogen), which are ring crystals having several vertices, for the first time.[22] These crystals

ACS Publications © XXXX American Chemical Society

A

dx.doi.org/10.1021/cg2004003 | *Cryst. Growth Des.* XXXX, XXX, 000–000

Figure 1. Structure of (left) needle-shaped and (right) ring-shaped crystals. As a result of expansion and contraction, dislocations are generated (⊥ symbols).
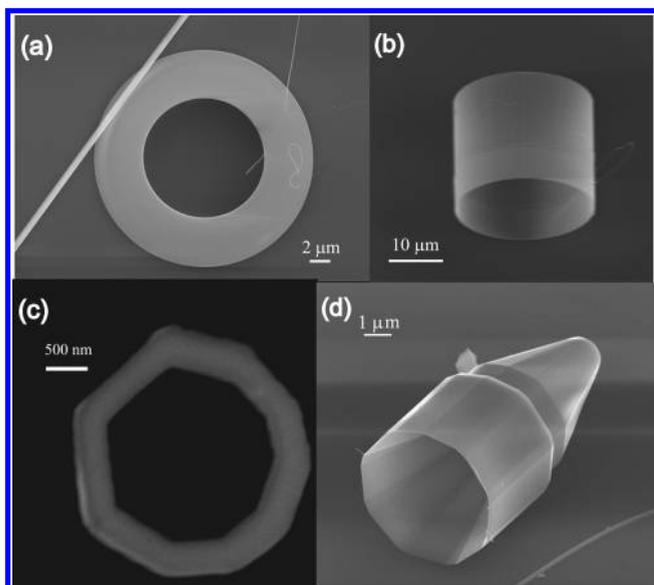
Figure 2. Topological crystals and polyhedral topological crystals of TaS₃. (a) Ring and (b) tube of smooth topological crystals. (c) Nonagon and (d) pencil-shaped polyhedral topological crystals.

were synthesized together with whiskers and ring crystals. Figure 2 shows typical topological crystals and polyhedral topological crystals. Whisker crystals are usually very thin, with typical thicknesses of 0.1−10 μm and lengths of 10 μm−1 cm, because of the quasi-one-dimensional crystal structure, where the basic structure of TaS₃ is a triangular prism whose structure is one metallic atom surrounded by six chalcogen atoms. The longest dimension is parallel to the axis of symmetry of the triangular prism. Our samples of TaS₃ belong to the orthorhombic system.[12] The crystal of TaS₃ displays $Pmn2_1$ space group symmetry.[23] The lattice constants were found to be $a = 36.804$ Å, $b = 15.177$ Å, and $c = 3.340$ Å. The c axis corresponds to the longest dimension. Ring/tube crystals, as shown in Figure 2a,b, had typical thicknesses of 0.1−100 μm, widths of 0.1−10 μm, and radii of 1−100 μm. The one-dimensional axis is parallel to the circumference.

Shown in Figure 2c,d are scanning electron microscopy images of typical polyhedral topological crystals. The dimensions of the polyhedral topological crystal in Figure 2c are 500 nm in width, 1.8 μm in radius, and 1 μm in thickness. The interior
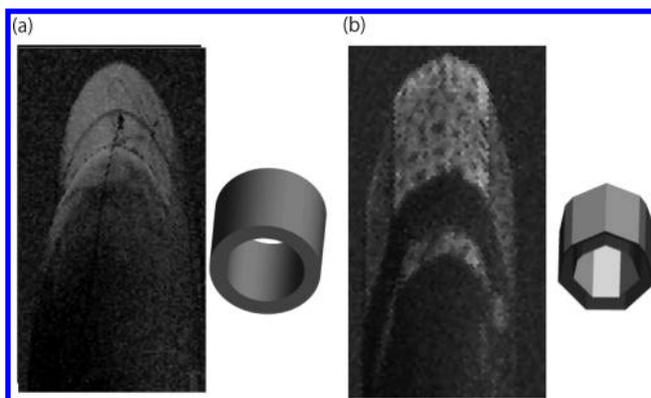
Figure 3. Intensity maps of (a) ring and (b) polyhedral crystals of EBSD obtained using field-emission scanning electron microscopy. The samples were observed from this perspective.

angles of the vertices are not equal. In the case of Figure 2c, the crystal is shaped as a nonagon, and in the case of Figure 2d, the radius of the crystal becomes gradually smaller from 4.5 to 1.0 μm, like a sharpened pencil.

We investigated the orientation of the crystal axes of the ring and polyhedral crystals as a function of position using electron backscatter diffraction (EBSD) patterns to confirm their crystallinity and the flatness of the facets. The spatial resolution of the EBSD patterns is several tens of nanometers, depending on the electron probe radius. We set up ring (Figure 3a) and polyhedral (Figure 3b) crystals. In Figure 3, the brightness in the map is proportional to the intensity of the EBSD pattern.[24] Note that the high-crystallinity area shows a high EBSD intensity. Figure 4 shows the crystal misorientation (difference in the orientation of facets) profile of two crystals, scanned along the green arrow. The blue line shows the variation in the orientation of the crystal axis from the initial point of the green circle, and the red line shows that from an adjacent point. The orientation of the facets changes smoothly in the ring crystal, whereas significant discrete jumps are observed at distances of 4, 5, 7, and 9 μm in the polyhedral crystal.

■ DISCUSSION

To elucidate the formation mechanism of the polyhedral structures, we investigated the size distribution of 32 topological crystals of TaS₃, including 7 polyhedral crystals and 25 ring/tube crystals. We measured their center radius R and width W. The distribution of the topological crystals is plotted in Figure 5. Each red square represents a polyhedral ring crystal, and each black circle represents a smooth ring crystal. Based on this plot, we became aware that the ring crystals with radii smaller than 2 μm became polyhedral ring crystals. This suggests that the radius must play an important role in the localization of dislocations.

We compared our results with the $R-W$ phase diagram of ring crystals predicted by Hayashi et al., who applied Ginzburg−Landau theory for superconductivity.[21] They predicted three phases for ring crystals. In phase I, the crystals are free of dislocations. In phase II, dislocations are introduced into the ring crystals to relax the bending energy. In phase III, because the defects are so dense, there is no interplane rigidity. They also predicted polygonization in phase II. In Figure 5, phase I is colored purple, phase II is blue and yellow, and phase III is red. The black area is the forbidden area for which $R < W$. To calculate the phase boundaries, we used the parameters of TaS₃[25,26] as γ^2
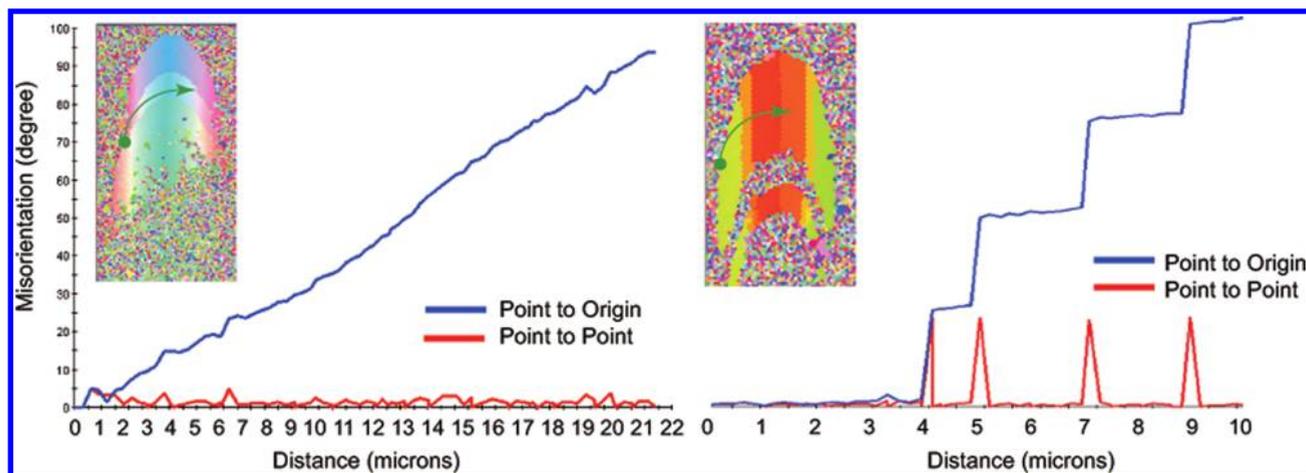
Figure 4. Misorientation profiles from an initial point (green circle) to green arrows for (left) ring and (right) polyhedral crystals. The blue line shows the variation in the orientation from the initial point of the green circle, and the red line shows that from an adjacent point. The insets show the orientations of the crystal axis on each point. The area of the same color corresponds to the same orientation of the crystal axis.
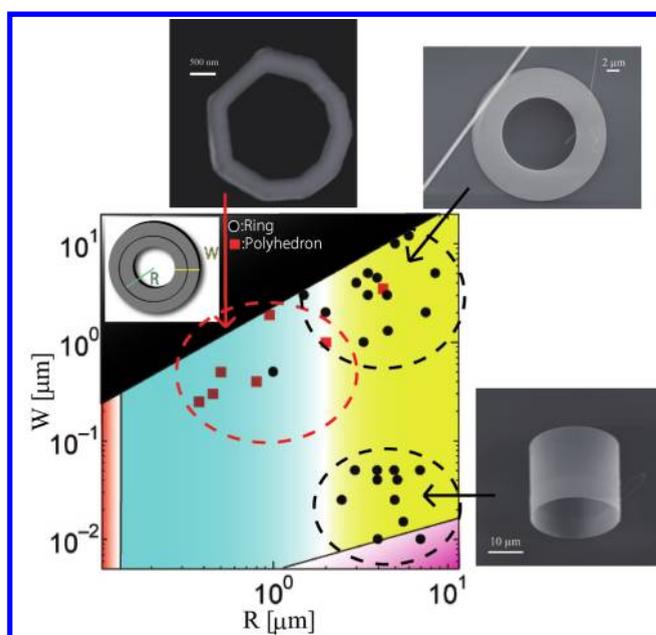

Figure 5. Phase diagrams of topological crystals showing the dependence of the radius and width. Red squares indicate polyhedral crystals, and black circles indicate ring crystals. The black area shows the range in which ring-crystal formation is forbidden. The other three areas divided by two black lines are based on Hayashi et al.'s theory. When the radius is smaller than 2 μm, the crystals become polyhedrons. The boundary between polyhedral and ring crystals is indicated by a white line.

$\approx 10^{-2}$, $d_x = 0.3$ nm, and $d_y = 2$ nm for the equations $R_{c1} = \pi W^2 / 2\gamma d_y$ and $R_{c2} = 2\pi d_y^2 / \gamma d_x$ in ref 21, where γ^2 is Young's modulus divided by shear modulus, d_x is the lattice constant in the x direction, and d_y is the lattice constant in the y direction. The boundary radius R_{c2} dividing phase III and phase II is equal to 133.3 nm, and the boundary radius R_{lim}, which is equal to the smallest value of R_{c1}, dividing phase II and phase I is equal to 1138 nm. The boundary R_{lim} corresponds approximately to the ring-tube boundary of our results. Hence, the tube crystals correspond to a clear circle without defects. In the case of ring crystals containing edge dislocations, the arrangement of them is

nontrivial and is not confirmed. We found that the crystals mostly became polyhedral crystals for $R < 2 \mu$m in the $R-W$ diagram. In consequence, we drew a boundary between the polyhedral and ring crystal areas, indicated by the white line between the blue and yellow areas in Figure 5. In the end, Figure 5 is divided into four areas; red, purple, blue, and yellow. We discovered experimentally that the vertices are inherent in ring crystals and that the phase transition from ring to polyhedral crystals is caused by the variation in radius size.

Our results suggest that the main factor in the polygonization is the radius-dependent interaction between the edge dislocations. Figure 6 shows the relationship between the interaction energy and the position of dislocations. The red symbols ($\perp$ symbols) represent positions of edge dislocations, and the black curves show the interaction energy.[27] When two dislocations move on the same crystal line or plane, a repulsive force is exerted between them. As a result of the dislocation motion, plastic deformation occurs at an edge of a bulk crystal to reduce the stress within it. The passage of a dislocation through a bulk crystal is equivalent to a slip displacement of one part of the bulk crystal. This is consistent with a bulk crystal, but in the case of topological crystals, the bulk model is not applicable. Topological crystals with a closed curve do not have an edge, and hence, slipping dislocations cannot exit from the crystal. When many dislocations are generated, cylinder-shaped walls of dislocations are expected to be formed as a result of the arrangement of the dislocations on parallel lines.[16,17] Here, we considered two dislocations moving on different crystal lines or planes. When the two dislocations are sufficiently far apart, a repulsive force is exerted; however, when the distance is short, an attractive force is exerted. As a result of the attractive interaction, the edge dislocations become concentrated on a vertical line. This is called a polygonization wall (Figure 7).[28,29] The average distance between dislocations becomes a function of R. Thus, for a constant number of edge dislocations, when the radius is large, a ring crystal is formed with a repulsive force, and when the radius is small, a polyhedral crystal is formed with an attractive force.

Because the polygonization is controlled by two parameters, our results are different from the structures of other multifaceted crystals obtained by self-assembly[30,31] in terms of the growth
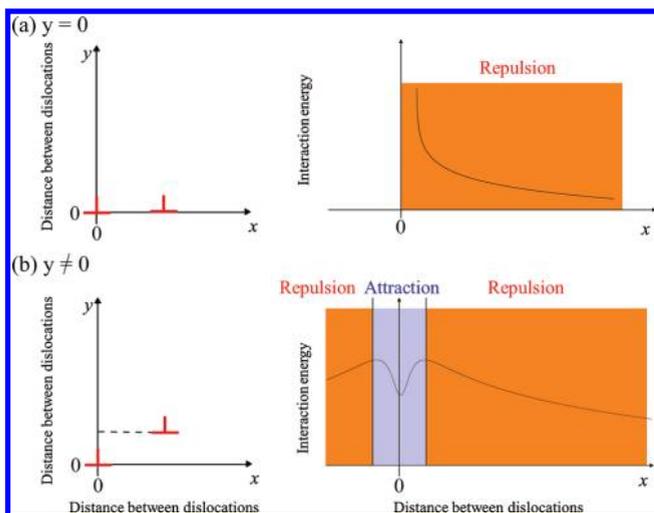
Figure 6. Interaction energy between the edge dislocations on (a) the same plane and (b) other planes shifting to the vertical (y) direction. The red symbols (⊥ symbols) and black lines show the edge dislocations and interaction energy in the x direction, respectively. At large distances, a repulsive force is exerted, and at short distances, an attractive force is exerted in the case of b.
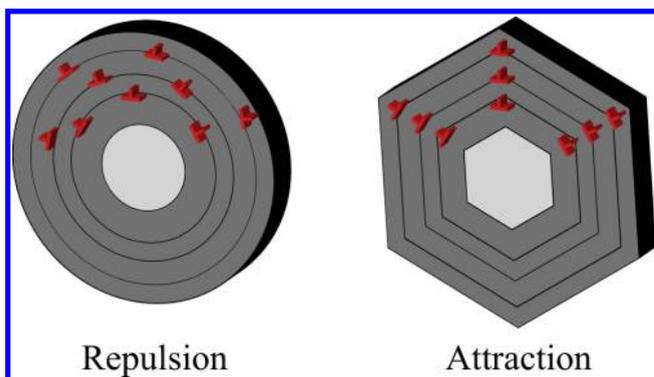
Figure 7. Polygonal walls resulting from the concentration of edge dislocations on a vertical line.

mechanism. Similar polyhedral nano- and microstructures were discovered in graphite in 2000.[32] A theoretical calculation of free energy indicated that their polygonization occurs in graphene sheets with diameters of less than 15 nm.[33] However, the polygonization of MX_3 topological crystals occurs on the micrometer scale. Forming corners from a whisker is entirely different from forming corners from a six-member carbon ring because the former configuration has a one-dimensional line and the latter configuration has a two-dimensional film. The polygonization of MX_3 ring crystals must be caused by a different mechanism. In this context, we believe that our discovery contains a novel research field of crystallography. The amount and positions of the defects within the crystal will be confirmed by the observation of topological phenomena.

■ CONCLUSIONS

In summary, we have discovered polyhedral topological crystals in the TaS_3 system. The formation mechanism is related to the edge dislocations arrayed on a vertical line by the distance-dependent interactions between them. We propose a polygonization phase in the width versus radius phase diagram for ring-shaped crystals.

■ AUTHOR INFORMATION

Corresponding Author
*E-mail: tsubota@eng.hokudai.ac.jp. Phone: +81 (11)706 7293. Fax: +81 (11)706 7293.

■ REFERENCES

(1) Kroto, H. W.; Heath, J. R.; O'Brien, S. C.; Curl, R. F.; Smalley, R. E. *Nature* **1985**, *318*, 162–163.
(2) Tenne, R.; Margulis, L.; Genut, M.; Godes, G. *Nature* **1992**, *360*, 444–446.
(3) Iijima, S. *Nature* **1991**, *354*, 56–58.
(4) Aharonov, Y.; Bohm, D. *Phys. Rev.* **1959**, *115*, 485–491.
(5) Bong, D. T.; Clark, T. D.; Granja, J. R.; Ghadiri, M. R. *Angew. Chem., Int. Ed.* **2001**, *40*, 988–1011.
(6) Zhou, L.; Wang, W.; Zhang, L.; Xu, H.; Zhu, W. *J. Phys. Chem. C* **2007**, *111*, 13659–13664.
(7) Hosten, O.; Kwiat, P. *Science* **2008**, *319*, 787–790.
(8) Tanda, S.; Kawamoto, H.; Shiobara, M.; Sakai, Y.; Yasuzuka, S.; Okajima, Y. *Physica B* **2000**, *284*, 1657–1658.
(9) Tanda, S.; Tsuneta, T.; Okajima, Y.; Inagaki, K.; Yamaya, K.; Hatakenaka, N. *Nature* **2002**, *417*, 397–398.
(10) Matsuura, T.; Yamanaka, M.; Hatakenaka, N.; Matsuyama, T.; Tanda, S. *J. Cryst. Growth* **2006**, *297*, 157–160.
(11) Matsuura, T.; Tanda, S.; Asada, K.; Sakai, Y.; Tsuneta, T.; Inagaki, K.; Yamaya, K. *Physica B* **2003**, *329*, 1550–1551.
(12) Tsubota, M.; Inagaki, K.; Tanda, S. *Physica B* **2009**, *404*, 416–418.
(13) Nobukane, H. *Private communication*, Hokkaido University, Sapporo, Japan, 2006.
(14) Shimatake, K.; Toda, Y.; Tanda, S. *Phys. Rev. B* **2006**, *73*, 153403-1–153403-4.
(15) Matsuura, T.; Tsuneta, T.; Inagaki, K.; Tanda, S. *Phys. Rev. B* **2006**, *73*, 165118-1–165118-5.
(16) Tsuneta, T.; Yamamoto, K.; Ikeda, N.; Nogami, Y.; Matsuura, T.; Tanda, S. *Phys. Rev. B* **2010**, *82*, 014105-1–014105-6.
(17) Matsuura, T.; Tsuneta, T.; Kumagai, G.; Tsubota, M.; Matsuyama, T.; Tanda, S. *Phys. Rev. B* **2011**, *83*, 174113-1–174113-5.
(18) Taylor, G. I. *Proc. R. Soc. A* **1934**, *145*, 362–405.
(19) Polanyi, M. *Z. Phys.* **1934**, *89*, 660–664.
(20) Orowan, E. *Z. Phys.* **1934**, *89*, 605–634.
(21) Hayashi, M.; Ebisawa, H.; Kuboki, K. *Eur. Phys. Lett.* **2006**, *76* (2), 264–270.
(22) Tsubota, M.; Toshima, T.; Hara, J.; Kumagai, G.; Hanzawa, H.; Ichimura, K.; Tanda, S. *Acta Crystallogr. A* **2008**, *64* (Suppl), C509.
(23) Kagoshima, S.; Nagasawa, H.; Sambongi, T. *One-Dimensional Conductors*; Springer-Verlag: Berlin, 1988.
(24) Schwartz, A. J.; Kumar, M.; Adams, B. L. *Electron Backscatter Diffraction in Materials Science*; Kluwer Academic/Plenum Publishers: New York, 2000.
(25) Xiang, X. D.; Brill, J. W. *Phys. Rev. B* **1987**, *36*, 2969–2971.
(26) Yamaya, K.; Oomi, G. *J. Phys. Soc. Jpn.* **1982**, *51*, 3512–3515.
(27) Read, W. T., Jr. *Dislocations in Crystals*, 3rd ed.; McGraw-Hill: New York, 1953.

D

dx.doi.org/10.1021/cg2004003 |*Cryst. Growth Des.* XXXX, XXX, 000–000

(28) Cottrell, A. H. *Dislocations and Plastic Flow in Crystals*; Clarendon Press: Oxford, U.K., 1953.

(29) Mott, N. F. *Proc. R. Soc. B* **1951**, *64*, 729–741.

(30) Medina, D. D.; Mastai, Y. *Cryst. Growth Des.* **2008**, *8*, 3646–3651.

(31) Pérez-Hernández, N.; Fort, D.; Pérez, C.; Martín, J. D. *Cryst. Growth Des.* **2011**, *11* (4), 1054–1061.

(32) Gogotsi, Y.; Libera, J. A.; Kalashnikov, N.; Yoshimura, M. *Science* **2000**, *290*, 317–320.

(33) Speck, J. S.; Endo, M.; Dresselhaus, M. S. *J. Cryst. Growth* **1989**, *94*, 834–848.